

## In-situ grown of FeCo<sub>2</sub>O<sub>4</sub> onto 2D-Carbyne coated nickel foam - A newer nanohybrid electrode for high performance supercapacitor

10 Preethi Dhandapani<sup>a</sup>, BalakrishnanBalan<sup>a</sup>, Tandabany Dinadayalane<sup>b</sup>,  
11 Subramania Angaiah<sup>a\*</sup>

14 <sup>a</sup>Electro-Materials Research Laboratory, Centre for Nanoscience and Technology,  
15 Pondicherry University, Puducherry, 605014, India

17 <sup>b</sup>Department of Chemistry, Clark Atlanta University, Atlanta, GA 30314, USA

21 \*Corresponding Author, E-mail: [a.subramania@gmail.com](mailto:a.subramania@gmail.com)

### Abstract

26 In this study, we synthesized carbyne by a simple chemical route and then this was coated  
27 on nickel foam. On this carbyne coated nickel foam, FeCo<sub>2</sub>O<sub>4</sub> was grown by the solvothermal  
28 process to serve as a nanohybrid electrode for supercapacitor applications. This nanohybrid  
29 electrode has shown high specific capacitance due to the large surface area, high electrical  
30 conductivity and improved rate characteristics. The specific capacitance of FeCo<sub>2</sub>O<sub>4</sub> @ Carbyne  
31 nanohybrid electrode was about 2584.8 Fg<sup>-1</sup> at the current density of 3 Ag<sup>-1</sup>. Furthermore, the  
32 asymmetric supercapacitor device integrated with FeCo<sub>2</sub>O<sub>4</sub> @ Carbyne and activated carbon  
33 (FeCo<sub>2</sub>O<sub>4</sub> @ Carbyne || AC) shows better performance with an energy density of about 96.59 Wh  
34 Kg<sup>-1</sup> at a high-power density of 2.25 kW kg<sup>-1</sup> with a capacitance decay of about 14.52 % even at  
35 5000 cycles. These outcomes provide a new approach for the development of supercapacitors  
36 with superior characteristics.

### KEYWORDS

49 FeCo<sub>2</sub>O<sub>4</sub>, Carbyne, Nanohybrid electrode, Solvothermal process, Supercapacitor, Specific  
50 capacitance.

1  
2  
3  
4  
5  
6  
7 **INTRODUCTION**

8  
9 Due to continuous increase in global population, energy crises have become one of the  
10 most crucial problems and it is mainly due to the over usage of conventional resources[1].  
11 Confronted with a serious problem of energy crises and environmental pollution, the desire for  
12 fabricating green and renewable energy sources is becoming significantly important[2,3].In such  
13 a case, energy harvesting and energy storage are used as technology. Among the devices  
14 developed for better energy harvesting and energy storage, battery and supercapacitor have been  
15 used extensively[4,5]. In general, batteries are energy storage devices in which reversible  
16 electrochemical reaction allows the storage of electrical energy as Columbic potential and  
17 releases the energy on demand, but with a limited life cycle[6]. The efforts toward increasing the  
18 life cycle of batteries led to the invention of supercapacitors[7],[8]. Of various known energy  
19 storage devices, the supercapacitor works and stores energy either based on the electrochemical  
20 double layer or pseudocapacitor effect[9]. The electrode materials for electrochemical double  
21 layer capacitor (EDLC)are carbon-based materials such as graphite, carbon nanotubes (CNTs),  
22 and graphene, which has large surface area and normally form a double layer at the  
23 electrode/electrolyte interface[10],[11]. On the other hand, pseudocapacitance which arises from  
24 the reversible faradaic redox process provides enhanced electrocapacitive performance compared  
25 to EDLC's effect. The used electrodes can be of conducting polymers, metal oxides, hydroxides,  
26 and transition metal oxides[12]. However, the decreased rate capability is due to lower electron  
27 transport that limits the usage of transition metal oxides[13]. This can be overcome by making  
28 use of mixed transition metal oxides ( $MCo_2O_4$ , where  $M = Ni, Fe, Sn, Mn, Cu$ ).  
29  
30  
31  
32  
33  
34  
35  
36  
37  
38  
39  
40  
41  
42

43 Owing to their multiple oxidation states, mixed transition metal oxide electrodes are  
44 attracted current interest for the enhanced electrochemical performance than the electrodes of  
45 individual transition metal oxides[14][15]. Of various mixed transition metal oxides,  $FeCo_2O_4$   
46 has much valuable positivity such as low cost, environmentally friendly, less toxicity, wide  
47 availability, better electronic conductivity and higher capacitance, which have fascinated much  
48 attention. Besides the mechanism, the surface phenomena hold a significant place. The surface  
49 phenomena of the material such as a larger surface area and suitable porous structure lead to the  
50 higher capacitance which facilitates electron transport and shortens the transmission distance.  
51 Hence, the researchers are focusing on developing the electrode material on the three-  
52 dimensional conducting surface such as Ni foam[16]. Recently, NF@NCO/NCO NFA  
53  
54  
55  
56  
57  
58  
59  
60  
61  
62  
63  
64  
65

1  
2  
3  
4 nanocomposite prepared by Kumar et al. exhibits a specific capacitance of about 2314 Fg<sup>-1</sup>  
5 corresponding to 2 mAcm<sup>-2</sup> with excellent cyclic stability[17]. Further, Zhang et al. fabricated  
6 mesoporous spinel NiCo<sub>2</sub>O<sub>4</sub> via a hydrothermal process that exhibits a specific capacitance of  
7 about 1619.1 Fg<sup>-1</sup> at 2 Ag<sup>-1</sup>[18]. Meanwhile, Yua et al. fabricated NiCo<sub>2</sub>O<sub>4</sub> on nickel foam which  
8 results in a better performance of about 1450 Fg<sup>-1</sup> at 20 Ag<sup>-1</sup> [19]. Though various mixed  
9 transition metal oxides are available, the usage of FeCo<sub>2</sub>O<sub>4</sub> as electrode had been rarely reported.  
10 For example, Nilesh et al. fabricated FeCo<sub>2</sub>O<sub>4</sub> nanowires which exhibit specific capacitance of  
11 1963 Fg<sup>-1</sup> in neutral electrolyte[20]. Similarly, Saad et al. fabricated FeCo<sub>2</sub>O<sub>4</sub> nanoflakes which  
12 exhibits specific capacitance of 433 Fg<sup>-1</sup> at 0.1 Ag<sup>-1</sup> in non-aqueous electrolyte. However, the  
13 specific capacitance exhibited by FeCo<sub>2</sub>O<sub>4</sub> electrode is low because of lower ion diffusion rate  
14 which results in limited diffusion at the electrode/electrolyte interface. This can be overcome by  
15 employing Carbyne which enhances the ion diffusion length by providing high surface  
16 area[21].Besides the well-known form of Carbon namely diamond and graphite, the new  
17 allotropes of Carbon named Carbyne has been reported[22].Carbyne are carbon atoms with  
18 either single and triple bond or double bond over the linear chain. These carbyne has high  
19 flexibility, superior strength and chemically stable in nature with the bandgap of about 2.56  
20 eV[23]. Thus, these properties open up a way for supercapacitor applications. Herein, we  
21 prepared carbyne by a simple chemical route and then this was coated on nickel foam. On this  
22 carbyne coated nickel foam, FeCo<sub>2</sub>O<sub>4</sub> was grown by the solvothermal process to use as a  
23 nanohybrid electrode for supercapacitors. FeCo<sub>2</sub>O<sub>4</sub>@Carbyne is of much interest because Fe<sup>2+</sup>  
24 with variable valence state is more active than Ni<sup>2+</sup> resulting in increased specific capacitance  
25 and it has been rarely reported[24]. Carbyne when made nanohybrid with FeCo<sub>2</sub>O<sub>4</sub>, it provides  
26 enhanced electrochemical performance because of its enhanced surface area. Later, the physical  
27 and electrochemical characterizations of FeCo<sub>2</sub>O<sub>4</sub>@Carbyne nanohybrid were examined.  
28  
29  
30  
31  
32  
33  
34  
35  
36  
37  
38  
39  
40  
41  
42  
43  
44  
45  
46  
47  
48  
49

## 50 EXPERIMENTAL SECTION

### 51 Chemicals Used

52 Silver nitrate, ammonia and benzene were purchased from Sigma Aldrich USA.  
53 Perchloric acid, FeCl<sub>3</sub>.4H<sub>2</sub>O, Co (NO<sub>3</sub>)<sub>2</sub>.6H<sub>2</sub>O, urea and ethylene glycol were purchased from  
54 Merck, India. Distilled water was utilized throughout the reaction.  
55  
56  
57  
58  
59  
60  
61  
62  
63  
64  
65

1  
2  
3  
4  
5  
6  
7 **Preparation of Carbyne**

8  
9 Initially, 0.4 g of silver nitrate was dissolved in 100ml of aqueous ammonia solution  
10 using a magnetic stirrer for 10 min. Later, 50ml of benzene was added to the above solution and  
11 then 2.5 g of calcium carbide was added until a uniform mixture was obtained. Further 3 mol/L  
12 of the perchloric acid was added to the above mixture until the nature of the solution becomes  
13 acidic. Once, the state of the solution became acidic, the reaction was kept under undisturbed  
14 conditions for 12 hours. Finally, the reaction mixture was filtered, washed and dried under  
15 vacuum at 70 °C for four hours.  
16  
17

18  
19 **Preparation of FeCo<sub>2</sub>O<sub>4</sub>@Carbyne nanohybrid**

20  
21 First, the nickel foam was cleaned thoroughly to remove oxides and dirt present on it.  
22 **Figure1** depicts the schematic sketch of FeCo<sub>2</sub>O<sub>4</sub> @Carbyne nanohybrid. The nickel foam was  
23 immersed in 3M HCl solution for 10 min under sonication. Then, it was cleaned and dried for 30  
24 mins. The treated nickel foam was then coated with the as-prepared carbyne and subjected to  
25 drying at 50 °C for two hours in the oven. Later, the solution containing 1mmol of FeCl<sub>3</sub>.4H<sub>2</sub>O,  
26 2mmol of Co (NO<sub>3</sub>)<sub>2</sub>.6H<sub>2</sub>O and 50mmol of urea was prepared by dissolving them in a solution  
27 containing 30ml of ethylene glycol and 10ml of distilled water under stirring for 30min. This  
28 reaction solution was then poured into 100ml of an autoclave. To this, carbyne-coated nickel  
29 foam was immersed and maintained in a furnace at 200 °C for 24 hours to grow FeCo<sub>2</sub>O<sub>4</sub> onto  
30 carbyne coated nickel foam. This autoclave was taken out and allowed to cool naturally. Then,  
31 the carbyne coated nickel foam was separated and dried at 60 °C for 3 hours to get FeCo<sub>2</sub>O<sub>4</sub>  
32  
33  
34  
35  
36  
37  
38  
39  
40  
41  
42  
43  
44  
45  
46  
47  
48  
49  
50  
51  
52  
53  
54  
55  
56  
57  
58  
59  
60  
61  
62  
63  
64  
65

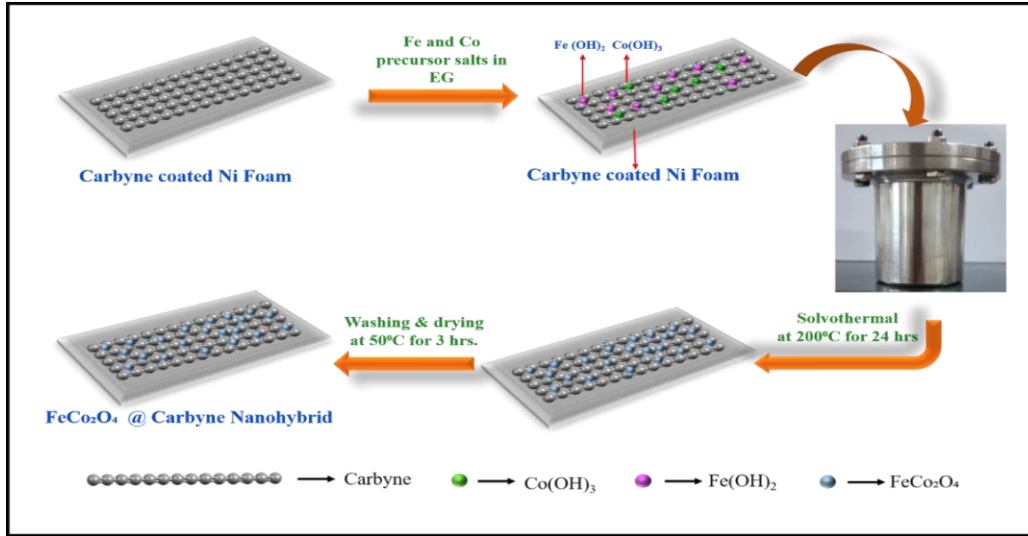


Figure 1 Schematic sketch of the synthesis of  $\text{FeCo}_2\text{O}_4$ @Carbyne electrode

## Physical Characterization

The structure and crystallinity of  $\text{FeCo}_2\text{O}_4$ @Carbyne nanohybrid was obtained by using an x-ray diffraction (XRD) analyzer (Rigaku, Model: Ultima IV) with a wavelength of  $1.540\text{ \AA}$  at the scan rate of  $5^\circ$  to  $80^\circ$  with an increment of  $0.05^\circ$ . The micro-Raman spectrometer (Renishaw RW-2000) employing  $\text{Ar}^+$  laser with the wavelength of  $514\text{ nm}$  was employed to analyze the Raman spectra. The morphology of the prepared nanostructure was investigated using field emission scanning electron microscopy studies (Carl Zeiss; Model: Sigma). In addition, the presence of elements was confirmed by energy dispersive X-ray analysis (EDAX) analysis (BRUKER). The oxidation state of the prepared nanostructure was recorded using an Ultra DLD X-ray photoelectron spectrometer (XPS) with an operating power of about  $75\text{ W}$ .

## Electrochemical Characterization

The electrochemical characterization was conducted using a three-electrode set up employing  $\text{FeCo}_2\text{O}_4$ @Carbyne, platinum and saturated calomel as the working, counter and reference electrode in  $3\text{M KOH}$  electrolyte using the electrochemical analyzer (Biologic Model: VSP). The cyclic voltammetry test was performed in the potential range of  $-0.5$  to  $0.3\text{V}$  for scan rates ranging from  $5$ – $100\text{ mVs}^{-1}$ . The galvanostatic charge-discharge test was done in the potential of  $-0.3$  to  $0.3\text{V}$  for a current density of  $3$ ,  $5$ ,  $7$  and  $10\text{ Ag}^{-1}$ . The Electrochemical Impedance Spectroscopy (EIS) studies were carried out in the frequency range of  $100\text{ kHz}$  to

1Hz with an amplitude of 10mV. From the GCD curve, the specific capacitance was calculated using the formula;[25]

$$C_{sp} = \frac{I (\Delta t)}{m (\Delta V)} \quad \dots \quad (1)$$

Where,  $I$  indicates current (A),  $\Delta t$  indicates discharging time (secs),  $m$  indicates the mass of electrode (g),  $\Delta V$  indicates potential difference(V).

Furthermore, the ASC device was assembled using a positive electrode made of FeCo<sub>2</sub>O<sub>4</sub>@Carbyne nanohybrid, a negative electrode made of activated carbon, and a separator made of PVDF polymer membrane soaked in 3M KOH. Later, the optimum mass ratio between both electrodes was calculated using the equation;[26]

$$\frac{m_+}{m_-} = \frac{C_- \Delta V_-}{C_+ \Delta V_+} \quad \dots \quad (2)$$

Where,  $C_+$  and  $C_-$  indicate the specific capacitance (Fg<sup>-1</sup>) of both electrodes,  $\Delta V_+$  and  $\Delta V_-$  as the potential difference (V) of both electrodes, respectively. Meanwhile, the energy density and power density are obtained using the below equation;[27]

$$\text{Energy Density} = \frac{C V^2}{2} \quad \dots \quad (3)$$

$$\text{Power Density} = \frac{E_{cell} \times 3600}{\Delta t} \quad \dots \quad (4)$$

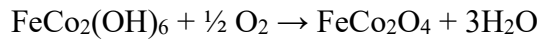
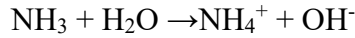
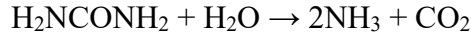
Where,  $E_{cell}$  indicates the energy density of the cell (Wh kg<sup>-1</sup>),  $\Delta t$  indicates discharge time (mins).

## RESULTS AND DISCUSSION

### Mechanism for the formation of FeCo<sub>2</sub>O<sub>4</sub> nanoparticles

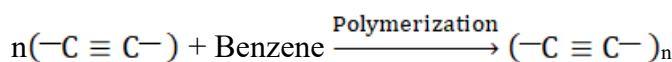
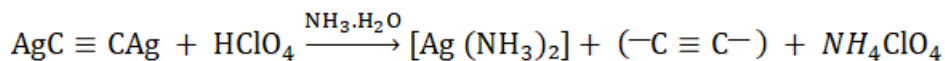
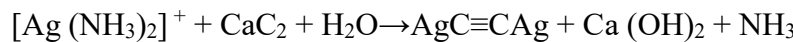
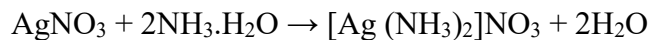
During the solvothermal process, at the initial state hydrolysis of urea occurs with the liberation of ammonia and the OH<sup>-</sup> ions. These OH<sup>-</sup> ions react with metal cations to form the

1  
2  
3  
4 mixed metal hydroxide,  $\text{FeCo}_2(\text{OH})_6$ . This mixed metal hydroxide,  $\text{FeCo}_2(\text{OH})_6$  upon further  
5 thermal treatment converted into  $\text{FeCo}_2\text{O}_4$  nanoparticles.[28]  
6  
7  
8  
9



14  
15  
16  
17 **Mechanism for the formation of Carbyne**

18 Initially, silver nitrate reacts with aqueous ammonia to form diamminesilver(I) nitrate which is  
19 then converted into a silver diamine complex. This diamine complex reacts with calcium carbide  
20 to form silver acetylide with the evolution of ammonia and calcium hydroxide. Later, the formed  
21 silver acetylide undergoes decomposition in presence of perchloric acid and aqueous ammonia  
22 solution to form  $(-\text{C}\equiv\text{C}-)_n$  which is further undergone polymerization to form carbyne. During  
23 this reaction, the formed ammonia and calcium hydroxide are neutralized by perchloric acid. The  
24 generated carbyne dissolved in benzene leading to the formation of carbyne with a longer chain.  
25  
26  
27  
28  
29  
30  
31  
32  
33  
34  
35



46 From **Figure 1a** the diffraction peaks at 21.03, 31.3, 44.8, 55.8, 59.5 and 65.4 correspond  
47 to planes at (111), (220), (311), (422), (511) and (440) which are assigned to  $\text{FeCo}_2\text{O}_4$  with  
48 cubic structure (Fd3m space group) according to JCPDS card No: 98-009-8552 which are  
49 designated as  $[\text{A}(\text{B}'_2)]\text{O}_4$ [29]. In general, the formula  $[\text{A}(\text{B}'_2)]\text{O}_4$  indicates the binary metal  
50 oxides where A and B' corresponds to the metal cations occupying the tetrahedral or octahedral  
51 sites. In addition, **Figure 1b** depicts the XRD pattern of carbyne. The major peaks at 29.54,  
52  
53  
54  
55  
56  
57  
58  
59  
60  
61  
62  
63  
64  
65

34.43, 37.19, 57.08, 63.21 and 64.30 correspond to the planes at (002), (110), (111) and (113) with the hexagonal structure indicating the presence of carbyne according to the previous study[30]. All the diffraction peaks corresponding to both  $\text{FeCo}_2\text{O}_4$  and carbyne are present in  $\text{FeCo}_2\text{O}_4@\text{Carbyne}$  nanohybrid and it is shown in **Figure 1c**. Thus, the formation of  $\text{FeCo}_2\text{O}_4@\text{Carbyne}$  nanohybrid has been confirmed.

**Figure 1d** shows the Raman spectra of  $\text{FeCo}_2\text{O}_4$ , carbyne and  $\text{FeCo}_2\text{O}_4@\text{Carbyne}$ . In  $\text{FeCo}_2\text{O}_4@\text{Carbyne}$  nanohybrid, the presence of characteristic peaks at 519, 617 and 688  $\text{cm}^{-1}$  correspond to the  $E_g$ ,  $F_{2g}$  and  $A_{1g}$  vibrational modes of  $\text{FeCo}_2\text{O}_4$ . Meanwhile, the peaks at 1320 and 1569  $\text{cm}^{-1}$  indicate D and G bands of Carbyne, respectively[31]. Thus, the peaks corresponding to both Carbyne and  $\text{FeCo}_2\text{O}_4$  are present in the  $\text{FeCo}_2\text{O}_4@\text{Carbyne}$  nanohybrid.

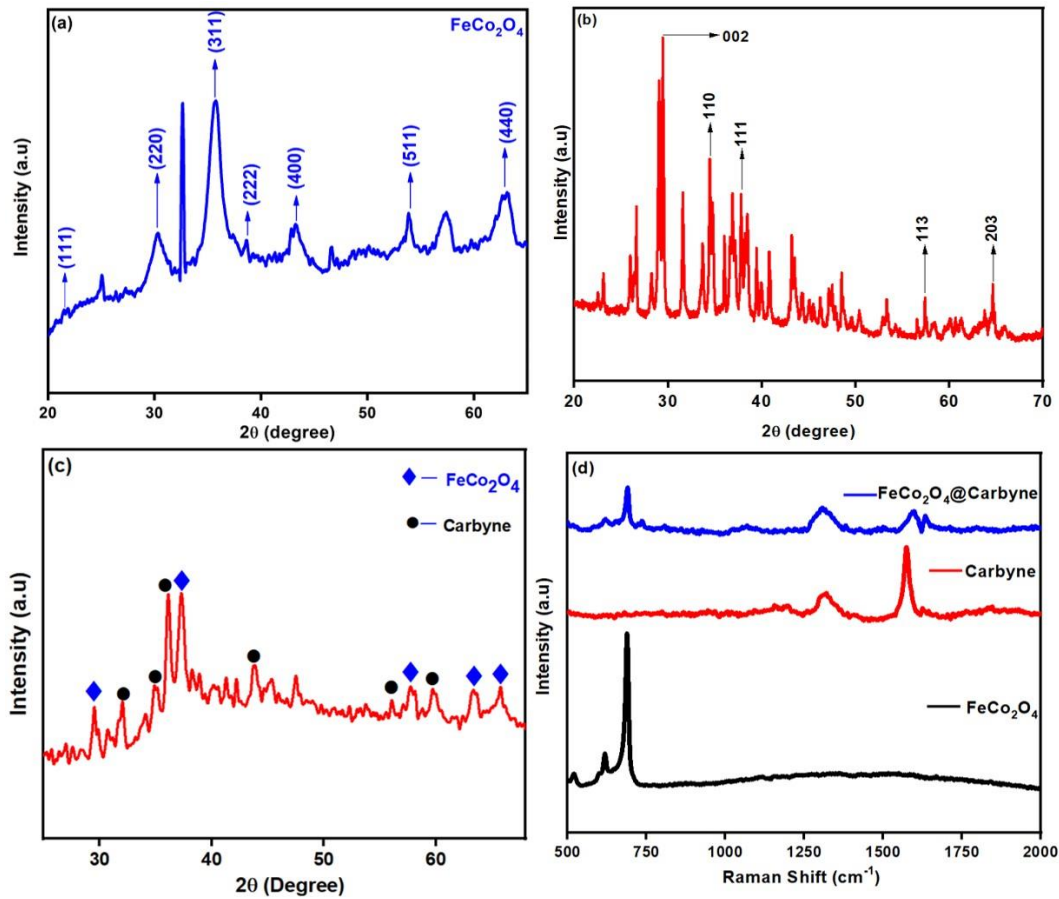
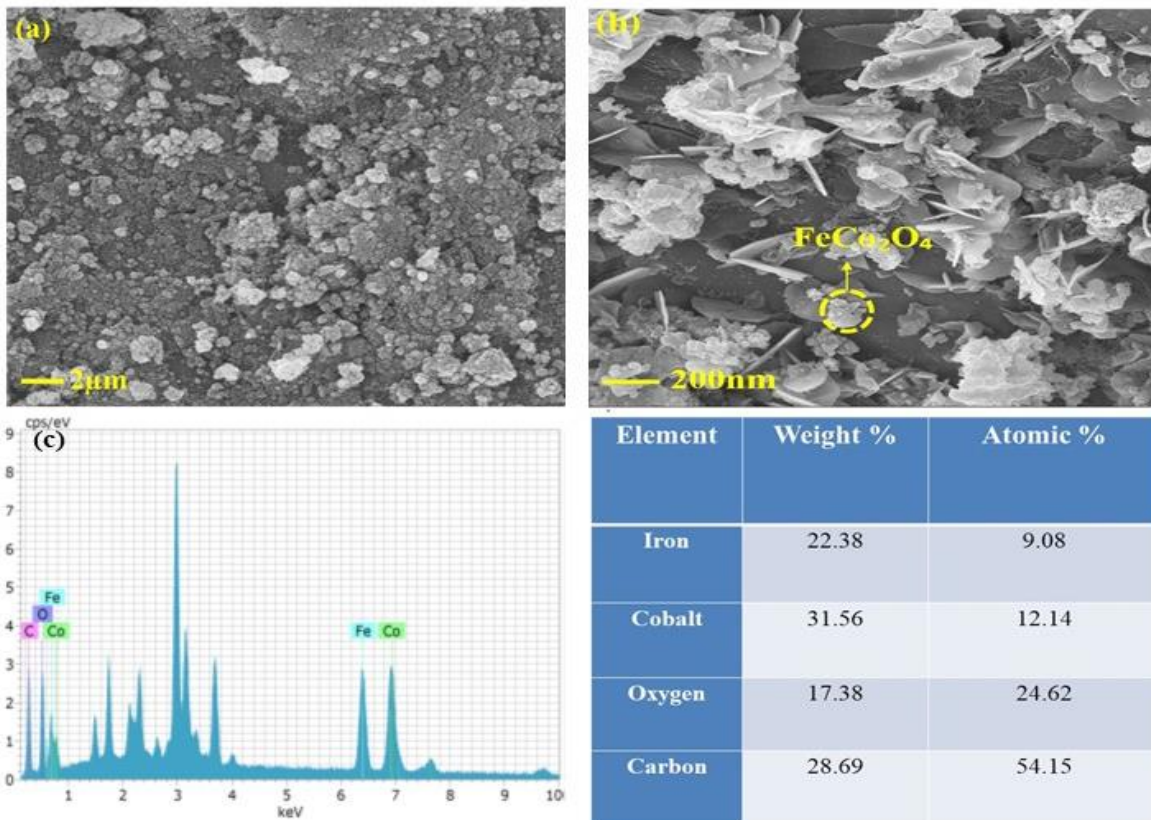


**Figure 1** XRD pattern of (a)  $\text{FeCo}_2\text{O}_4$ , (b) Carbyne, (c)  $\text{FeCo}_2\text{O}_4@\text{Carbyne}$  nanohybrid, (d) Raman spectra of  $\text{FeCo}_2\text{O}_4$ , Carbyne and  $\text{FeCo}_2\text{O}_4@\text{Carbyne}$  nanohybrid.

The morphologies of  $\text{FeCo}_2\text{O}_4$  and  $\text{FeCo}_2\text{O}_4@\text{Carbyne}$  nanohybrid were analyzed by FE-SEM analyzer. **Figure 2a** shows the morphology of as-synthesized  $\text{FeCo}_2\text{O}_4$  nanoparticles. Using image J software, the size of the nanoparticle is found to be  $\sim 36\text{nm}$ . In addition, the morphology of  $\text{FeCo}_2\text{O}_4@\text{Carbyne}$  nanostructure is shown in **Figure 2b**. From **Figure 2b**, it is observed that  $\text{FeCo}_2\text{O}_4$  nanoparticles are decorated onto the carbyne with nanoflake structure[32]. The carbyne with nanoflakes structure is grown uniformly on the nickel foam-forming petal-like structure. These nanoflake morphology results in the cross-linked structure providing good mechanical strength. Thus,  $\text{FeCo}_2\text{O}_4/\text{Carbyne}$  nanoflakes show better electrochemical performance arising from their improved surface area, larger electroactive sites and facilitate faster ion diffusion into the electrolyte. **Figure 2c** depicts the EDAX image of  $\text{FeCo}_2\text{O}_4@\text{Carbyne}$  nanohybrid. The EDAX spectra indicate the prominent peaks of elements present, which confirms that the prepared  $\text{FeCo}_2\text{O}_4@\text{Carbyne}$  electrode consists of Fe, Co, O<sub>2</sub> and C elements. The elements present and their weight percentage are tabulated.



1  
2  
3  
4 **Figure 2** FESEM image of (a) FeCo<sub>2</sub>O<sub>4</sub> and (b) FeCo<sub>2</sub>O<sub>4</sub>@Carbyne nanohybrid on Ni foam; (c)  
5 EDAX image of FeCo<sub>2</sub>O<sub>4</sub>@Carbyne nanohybrid and its elements present with weight and atomic  
6 percentages.  
7  
8

9 XPS measurements were used to analyze the surface and oxidation state of the produced  
10 FeCo<sub>2</sub>O<sub>4</sub>@carbyne nanohybrid. **Figure 3a** indicates the XPS spectra of Fe 2p with major peaks  
11 corresponding to binding energy values of 710.3eV and 723.1eV indicating Fe 2p<sub>3/2</sub> and Fe 2p<sub>1/2</sub>.  
12 In addition, the deconvoluted peaks at the binding energy values of 710.2eV and 722.8eV  
13 indicate the Fe<sup>2+</sup> while the peaks at 712.3eV and 725.4eV indicate Fe<sup>3+</sup>[29]. Thus, both Fe<sup>2+</sup> and  
14 Fe<sup>3+</sup> states coexist in FeCo<sub>2</sub>O<sub>4</sub>@carbyne. **Figure 3b** depicts the XPS spectra of Co 2p with  
15 major peaks at 779.4eV and 795.7eV indicating the presence of Co 2p<sub>3/2</sub> and Co 2p<sub>1/2</sub>. The  
16 presence of deconvoluted peaks at 781.5eV and 795.3eV corresponds to Co<sup>2+</sup>; while the peaks at  
17 780.1eV and 795.8eV correspond to Co<sup>3+</sup>. Thus, both Co<sup>2+</sup> and Co<sup>3+</sup> states coexist in the  
18 nanohybrid electrode. **Figure 3c** displays the XPS spectra of O 1s which consists of main peaks  
19 at 529.1eV and 531.4eV. The characteristic peak at 529.1eV corresponds to the metal-oxygen  
20 bond and the other peak at 531.4eV corresponds to oxygen in OH<sup>-</sup> groups[16]. **Figure 3d**  
21 indicates the XPS spectra of C 1s which are deconvoluted into several peaks. The strongest peak  
22 centered at 284.9eV corresponds to -C≡C-C≡C- carbyne background and the peak at 291.6eV  
23 corresponds to the shake-up satellite peak which arises from the aromatic compound[33].  
24  
25  
26  
27  
28  
29  
30  
31  
32  
33  
34  
35  
36  
37  
38  
39  
40  
41  
42  
43  
44  
45  
46  
47  
48  
49  
50  
51  
52  
53  
54  
55  
56  
57  
58  
59  
60  
61  
62  
63  
64  
65

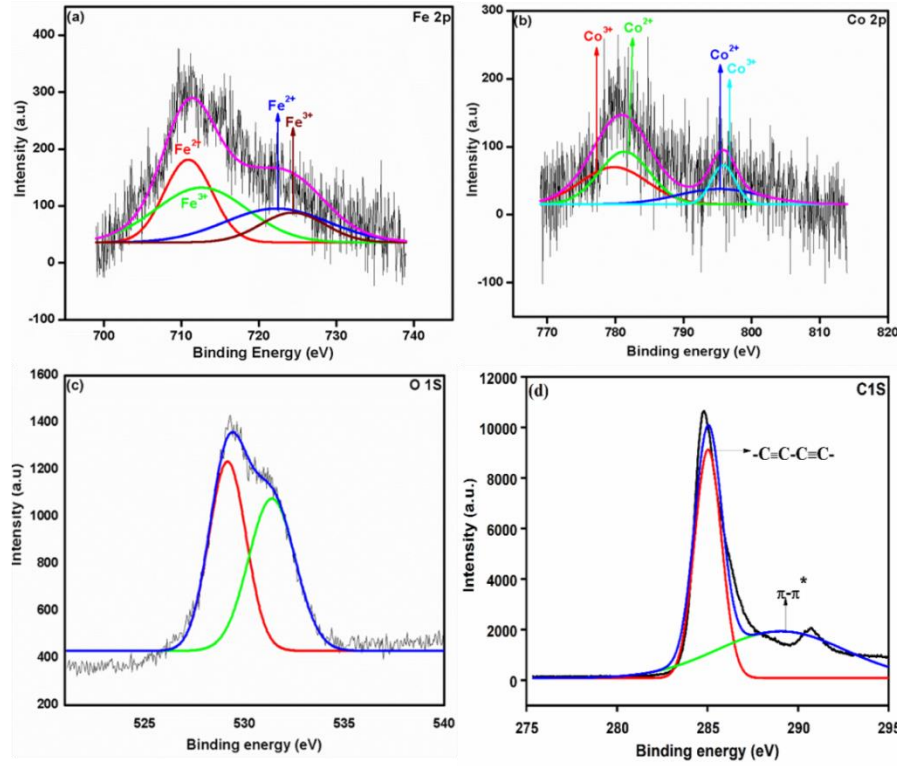


Fig.3 XPS spectrum of FeCo<sub>2</sub>O<sub>4</sub>@Carbyne (a)Fe 2p, (b) Co 2p, (c) O 1s and (d) C1s

To evaluate the electrochemical characteristics of prepared FeCo<sub>2</sub>O<sub>4</sub>@Carbyne nanohybrid, Cyclic Voltammetry, Galvanostatic Charge Discharge and Electrochemical Impedance Spectroscopy were performed. **Figure 4a** shows a typical CV curve of FeCo<sub>2</sub>O<sub>4</sub>, Carbyne and FeCo<sub>2</sub>O<sub>4</sub>@Carbyne electrodes obtained at the scan rate of 25mVs<sup>-1</sup>. From **Figure 4a** comparatively, the area enclosed by the FeCo<sub>2</sub>O<sub>4</sub>@Carbyne electrode is found to be higher than the carbyne and FeCo<sub>2</sub>O<sub>4</sub> electrode. This indicates FeCo<sub>2</sub>O<sub>4</sub>@Carbyne nanohybrid electrode maintains an increased specific capacitance than FeCo<sub>2</sub>O<sub>4</sub> and Carbyne electrodes. Besides the CV curve, it is found that carbyne undergoes EDLC behavior and FeCo<sub>2</sub>O<sub>4</sub> and FeCo<sub>2</sub>O<sub>4</sub>@Carbyne with non-rectangular shapes exhibit pseudocapacitive behavior.

**Figure 4b** elucidates the CV curve of FeCo<sub>2</sub>O<sub>4</sub>@Carbyne nanohybrid electrode obtained at different scan rates ranging from -0.5 to 0.3V. The quite different curve shape and redox peak of this electrode are not only demonstrating a pseudocapacitive nature but also reveals the addition of carbyne which plays a significant role in the electrochemical performance[22]. FeCo<sub>2</sub>O<sub>4</sub>@Carbyne nanohybrid has a typical faradaic electrochemical behavior rather than the

shape of EDLC. At a higher scan rate, the redox peak also increases revealing lower resistance of the electrode. From the CV curve, according to the power-law;

$$i = a\gamma^b \quad \dots \quad (5)$$

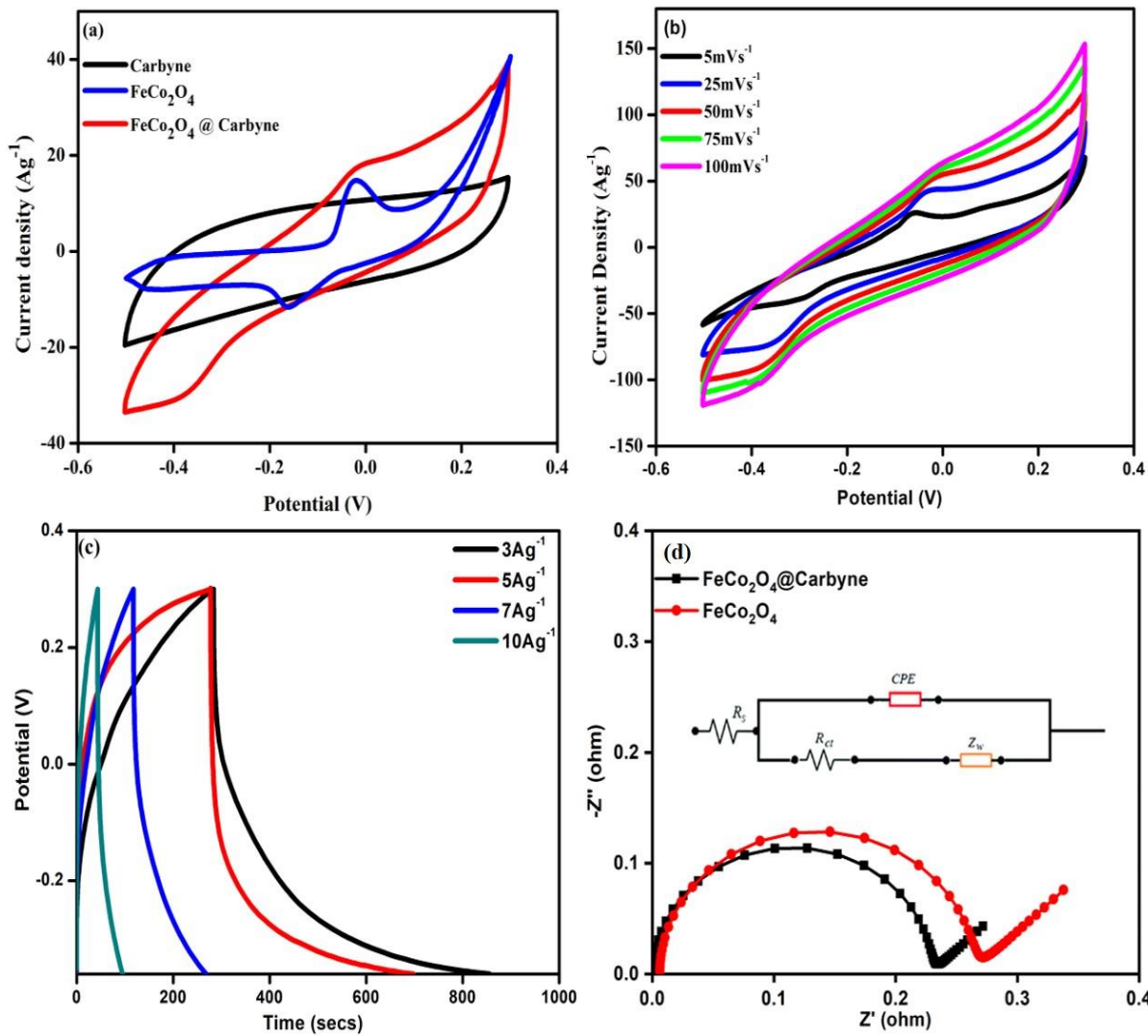
where  $i$  represents redox peak (A),  $\gamma$  represents scan rate and  $a$ ,  $b$  represents adjustable parameters, that are used to predict the type of the mechanism. The value of parameter  $b = 1$  indicates the capacitive controlled process, while  $b = 0.5$  represents diffusion-controlled process[34]. In the **inset of Figure 4b** the value of  $b$  from the redox peak was found to be 0.51, indicating that a diffusion-controlled process has occurred.

**Figure 4c** shows the galvanostatic charge-discharge curves of  $\text{FeCo}_2\text{O}_4@\text{Carbyne}$  nanohybrid operated between the working potential of -0.3 to 0.3V. As expected, the nanohybrid demonstrates a longer discharge time giving rise to a higher capacitance value. The specific capacitance is found to be as high as 2584.8, 2363.6, 1579.1 and 773.0  $\text{Fg}^{-1}$  at the current density of 3,5,7 and 10  $\text{Ag}^{-1}$ , respectively. Further, the presence of voltage plateaus in the GCD curve indicates the pseudocapacitive nature of the nanohybrid electrode which coincides well with the CV outputs. In addition, the symmetrical shape of the curve and the absence of iR drop reveals the excellent redox behavior with a lower internal resistance of the electrode. Table1 shows the comparison of as-prepared  $\text{FeCo}_2\text{O}_4@\text{Carbyne}$  nanohybrid electrodes with  $\text{FeCo}_2\text{O}_4$  and their nano-composites based electrodes reported earlier in the literature<sup>14,18,19,35,37</sup>.

**Table 1:** Comparison of specific capacitance of  $\text{FeCo}_2\text{O}_4@\text{Carbyne}$  based electrode with earlier reported results for  $\text{FeCo}_2\text{O}_4$  and its nano-composites.

Electrode Material	Specific Capacitance	Current Density	Electrolyte	Ref.
$\text{FeCo}_2\text{O}_4$ nanosheets	853.8 $\text{Fg}^{-1}$	5 $\text{Ag}^{-1}$	1M $\text{Na}_2\text{SO}_4$	[35]
$\text{FeCo}_2\text{O}_4$ nanowires	1963.0 $\text{Fg}^{-1}$	2 mA $\text{cm}^{-2}$	1M $\text{Na}_2\text{SO}_4$	[14]
$\text{FeCo}_2\text{O}_4$ nanoflakes	433.0 $\text{Fg}^{-1}$	0.1 $\text{Ag}^{-1}$	2M KOH	[18]
$\text{FeCo}_2\text{O}_4@\text{NiCo LDH}$	2426.0 $\text{Fg}^{-1}$	1 $\text{Ag}^{-1}$	2M KOH	[19]
$\text{FeCo}_2\text{O}_4 @ \text{MnO}_2$	2112.9 $\text{Fg}^{-1}$	40 mA $\text{cm}^{-2}$	2M KOH	[37]
<b><math>\text{FeCo}_2\text{O}_4@\text{Carbyne}</math></b>	<b>2584.2 <math>\text{Fg}^{-1}</math></b>	<b>3 <math>\text{Ag}^{-1}</math></b>	<b>3M KOH</b>	<b>This work</b>

Followed by CV and GCD,  $\text{FeCo}_2\text{O}_4@\text{Carbyne}$  nanohybrid electrode was subjected to EIS studies. **Figure 4d** shows EIS curves of  $\text{FeCo}_2\text{O}_4@\text{Carbyne}$  nanohybrid with two portions namely a semicircle followed by a vertical line. The smallest value of charge transfer resistance ( $R_{ct}$ ) obtained from the semicircle indicates that the electrode provides a larger active site and lower charge transfer resistance[38]. The presence of a straight line in the plot indicates the better capacitive behavior of the electrode with low diffusion resistance[39]. Consequently, the  $\text{FeCo}_2\text{O}_4@\text{Carbyne}$  nanohybrid provides charge transfer resistance ( $R_{ct}$ ) of about  $0.23\Omega$  which is smaller than  $\text{FeCo}_2\text{O}_4$  of about  $0.28\Omega$ . Thus, the results of EIS measurements reveal the easier transportation of electrolyte ions inside the nanohybrid electrode.



1  
2  
3  
4 **Figure4**(a)CV curves of  $\text{FeCo}_2\text{O}_4$ , Carbyne and  $\text{FeCo}_2\text{O}_4@\text{Carbyne}$  electrode corresponding to  
5 the scan rate of  $25\text{mVs}^{-1}$ , (b)CV curve of  $\text{FeCo}_2\text{O}_4@\text{Carbyne}$  electrode at different of 5, 25, 50,  
6 75 and  $100\text{ mVs}^{-1}$ , inset shows the **b**-value estimation from cathodic peak current of  
7  $\text{FeCo}_2\text{O}_4@\text{Carbyne}$  electrode, (c)GCD curve of  $\text{FeCo}_2\text{O}_4@\text{Carbyne}$  electrode, (d)Nyquist plots  
8 of  $\text{FeCo}_2\text{O}_4$  and  $\text{FeCo}_2\text{O}_4@\text{Carbyne}$ .  
9  
10  
11  
12  
13  
14

15 As a step forward considering the superior electrochemical performance, a supercapacitor  
16 was fabricated using  $\text{FeCo}_2\text{O}_4@\text{Carbyne}$ , activated carbon (AC) as a positive and negative  
17 electrode which is designated as  $\text{FeCo}_2\text{O}_4@\text{Carbyne} \parallel \text{AC}$ . To obtain the optimum mass ratio  
18 between the electrodes, the working potential of the CV studies of  $\text{FeCo}_2\text{O}_4@\text{Carbyne}$   
19 nanohybrid and the activated carbon is studied in 3M KOH electrolyte, respectively. From the  
20 mass balance theory, [the charge accumulated on the cathode is equal to the charge accumulated  
21 on the anode], the optimal mass ratio is calculated<sup>40,41</sup>. From the equation (2), the optimal mass  
22 ratio was found to be 0.54 (m<sup>+</sup>/m<sup>-</sup>).  
23  
24

25 **Figure 5a** depicts the CV curve of  $\text{FeCo}_2\text{O}_4@\text{Carbyne}$  and AC electrodes operated in the  
26 range of -1.2 to -0.2 V and -0.5 to 0.3 V at  $25\text{ mVs}^{-1}$ . The typical rectangular shape of the AC  
27 represents the EDLC behavior with no obvious redox peaks in the potential range of -1.2 to -0.2  
28 V; while the positive electrode exhibits redox peaks indicating its pseudocapacitive nature in the  
29 potential range of -0.5 to 0.3 V. Thus, the assembled asymmetric supercapacitor device is  
30 expected to be stable up to the operating potential of about 1.5 V. From the CV curve, the stable  
31 operating potential of the  $\text{FeCo}_2\text{O}_4@\text{Carbyne} \parallel \text{AC}$  cell is found to be around 1.5 V. **Figure 5b**  
32 shows the CV curve of the  $\text{FeCo}_2\text{O}_4@\text{Carbyne} \parallel \text{AC}$  obtained at scan rates of 5, 15, 25, 50, 75  
33 and  $100\text{ mVs}^{-1}$  in the range of 0 to 1.5 V. The non-rectangular shape of the CV curve indicates  
34 that the device undergoes both EDLC and pseudocapacitive behavior. In addition, at a higher  
35 scan rate, the area occupied by the curve seems to be increased and the uniformity of the CV  
36 curve was well maintained. The uniformity of the CV curve indicates the excellent capacitive  
37 behavior and reversibility of the electrodes. **Figure 5c** represents the GCD curve of the  
38  $\text{FeCo}_2\text{O}_4@\text{Carbyne} \parallel \text{AC}$  device obtained at different current densities. From the GCD curve, the  
39 specific capacitance was found to be  $309.11, 277.36, 252.12$  and  $230.41\text{ Fg}^{-1}$  at 3, 5, 7 and 10  
40  $\text{Ag}^{-1}$  respectively. The presence of voltage plateaus indicates that the device undergoes a  
41 Faradaic reaction which coincides well with CV curves. In addition, the curves are almost  
42  
43  
44  
45  
46  
47  
48  
49  
50  
51  
52  
53  
54  
55  
56  
57  
58  
59  
60  
61  
62  
63  
64  
65

1  
2  
3  
4 symmetric indicating good reversible electrochemistry of the fabricated device. Further, cycling  
5 stability is the key parameter that must be accounted for the fabricated device. **Figure 5d**  
6 represents the cyclic stability of the device conducted at the current density of  $10 \text{ Ag}^{-1}$  over 5000  
7 cycles. The specific capacitance of the device is well maintained during the initial cycles, which  
8 shows a decrease in the later cycles exhibiting capacitance retention of 85.48% over 5000 cycles.  
9 Even after a long life of 5000 cycles, the fabricated device maintained good reversibility with  
10 Coulombic efficiency of above 100% with undistorted and symmetric curves. Thus, the excellent  
11 capacitive behavior is due to the synergistic effect of both carbyne and  $\text{FeCo}_2\text{O}_4$  nanostructures.  
12  
13

14 To quantitatively analyze the interfacial performance at the electrode-electrolyte  
15 interface, an EIS test was conducted. **Figure 5e** elucidates the Nyquist plots of the device before  
16 and after 5000 cycles in the frequency range of 100 kHz to 1 Hz at an amplitude of 10 mV. The  
17 values of bulk solution resistance ( $R_s$ ) before and after 5000 cycles are found to be 1.06 and  
18 1.34, respectively. The value of  $R_s$  is obtained by real axis intercepts which arise due to, contact  
19 resistance of the electrode, electrolyte resistance and inherent resistance. Besides, to carry out a  
20 relation between energy and power density of the fabricated device, the Ragone plot is obtained.  
21 **Figure 5f** elucidates the Ragone plot of the fabricated device. The energy density of the  
22 fabricated device is found to be  $96.59 \text{ Wh kg}^{-1}$  at the power density of  $2.25 \text{ kW kg}^{-1}$ .  
23 Subsequently, even at the high current density of  $10 \text{ Ag}^{-1}$ , the energy density is well maintained  
24 up to  $72 \text{ Wh kg}^{-1}$  at the power density of about  $7.50 \text{ kW kg}^{-1}$ . The above outcomes reveal that the  
25 fabricated device suits for moderate energy density application due to its stability at both low and  
26 high current densities. The energy and power densities exhibited by  $\text{FeCo}_2\text{O}_4@\text{Carbyne} \parallel \text{AC}$   
27 device shows superior performance than other reported  $\text{FeCo}_2\text{O}_4$  and their composites such as  
28  $\text{FeCo}_2\text{O}_4@\text{MnO}_2 \parallel \text{AC}$  [ $22 \text{ Wh kg}^{-1}/0.40 \text{ kW kg}^{-1}$ ],  $\text{MnO}_2 \parallel \text{rGO/FeCo}_2\text{O}_4$  [ $46 \text{ Wh kg}^{-1}/3.60 \text{ kW kg}^{-1}$ ]  
29 and  $\text{FeCo}_2\text{O}_4 \parallel \text{FeCo}_2\text{O}_4$  [ $94 \text{ Wh kg}^{-1}/0.13 \text{ kW kg}^{-1}$ ].  
30  
31  
32  
33  
34  
35  
36  
37  
38  
39  
40  
41  
42  
43  
44  
45  
46  
47

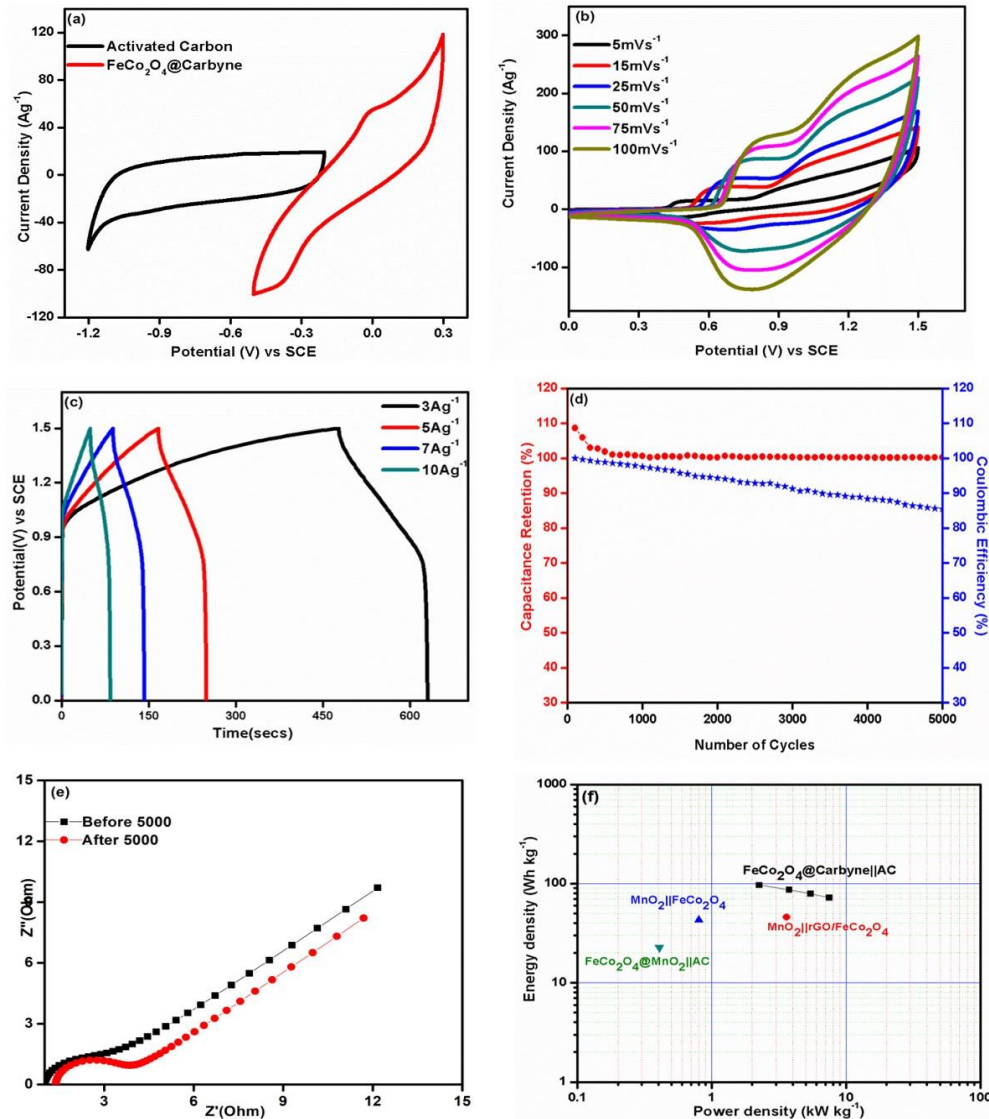


**Figure 5** (a) CV curves of  $\text{FeCo}_2\text{O}_4$ @Carbyne and activated carbon electrode at the scan rate of  $50\text{mVs}^{-1}$ , (b) CV curves of the supercapacitor device obtained at various scan rates, (c) GCD curves of the supercapacitor device obtained at various current densities, (d) Cyclic stability of supercapacitor device, (e) Nyquist plots of supercapacitor device before and after 5000 cycles, (f) Ragone plots

## CONCLUSION

In summary,  $\text{FeCo}_2\text{O}_4$ @Carbyne nanohybrid is synthesized by a two-step method to serve as an efficient electrode for supercapacitors. The crystallinity of the  $\text{FeCo}_2\text{O}_4$ @Carbyne nanohybrid electrode was confirmed by XRD analysis. The morphology of  $\text{FeCo}_2\text{O}_4$ @Carbyne

1  
2  
3  
4 is investigated by FE-SEM analysis. Due to the combined effect of both Carbyne and FeCo<sub>2</sub>O<sub>4</sub>,  
5 the FeCo<sub>2</sub>O<sub>4</sub>@Carbyne nanohybrid results in a specific capacitance of about 2584.77 Fg<sup>-1</sup> in 3M  
6 KOH electrolyte with superior electrochemical performance. Further, the fabricated device  
7 namely FeCo<sub>2</sub>O<sub>4</sub>@Carbyne||AC exhibits a higher specific capacitance of 309.1 Fg<sup>-1</sup> with  
8 excellent cyclic stability. In addition, it offers an energy density of 96.59 Wh kg<sup>-1</sup> corresponding  
9 to the power density of 2.25 kWkg<sup>-1</sup>. Thus, the increased capacitive characteristics of  
10 FeCo<sub>2</sub>O<sub>4</sub>@Carbyne overlaid a way for their usage in supercapacitor applications.  
11  
12  
13  
14  
15

16  
17  
18  
19 **CONFLICT OF INTEREST**  
20  
21

22 The authors declare no conflict of interest.  
23  
24

25  
26 **ACKNOWLEDGMENTS**  
27  
28

29 AS gratefully acknowledges the UGC, New Delhi for their financial support under the BSR Mid-  
30 Career Award Scheme (No. F.19- 214/2018). TD acknowledges the United States National  
31 Science Foundation for the funding through EiR (DMR-2100946) and PREM (DMR-2122147)  
32 Awards.  
33  
34  
35

36 **REFERENCES**  
37  
38

[1] M. Pathak, J.R. Jose, B. Chakraborty, C.S. Rout, High performance supercapacitor  
39 electrodes based on spinel NiCo<sub>2</sub>O<sub>4</sub>@MWCNT composite with insights from density  
40 functional theory simulations, *J. Chem. Phys.* 152 (2020).  
41  
42 <https://doi.org/10.1063/1.5138727>.  
43  
44 [2] N.R. Chodankar, H.D. Pham, A.K. Nanjundan, J.F.S. Fernando, K. Jayaramulu, D.  
45 Golberg, Y.K. Han, D.P. Dubal, True Meaning of Pseudocapacitors and Their  
46 Performance Metrics: Asymmetric versus Hybrid Supercapacitors, *Small.* 16 (2020) 1–35.  
47  
48 <https://doi.org/10.1002/smll.202002806>.  
49  
50 [3] D.P. Dubal, N.R. Chodankar, D.H. Kim, P. Gomez-Romero, Towards flexible solid-state  
51 supercapacitors for smart and wearable electronics, *Chem. Soc. Rev.* 47 (2018) 2065–  
52 2129. <https://doi.org/10.1039/c7cs00505a>.  
53  
54 [4] X. Lu, M. Yu, G. Wang, Y. Tong, Y. Li, Flexible solid-state supercapacitors: Design,  
55  
56  
57  
58  
59  
60  
61  
62  
63  
64  
65

1  
2  
3  
4 fabrication and applications, *Energy Environ. Sci.* 7 (2014) 2160–2181.  
5 https://doi.org/10.1039/c4ee00960f.  
6  
7 [5] X. Wang, X. Lu, B. Liu, D. Chen, Y. Tong, G. Shen, Flexible energy-storage devices:  
8 Design consideration and recent progress, *Adv. Mater.* 26 (2014) 4763–4782.  
9 https://doi.org/10.1002/adma.201400910.  
10  
11 [6] M. Winter, R.J. Brodd, What are batteries, fuel cells, and supercapacitors?, *Chem. Rev.*  
12 104 (2004) 4245–4269. https://doi.org/10.1021/cr020730k.  
13  
14 [7] P. Simon, Y. Gogotsi, B. Dunn, Where do batteries end and supercapacitors begin?,  
15 *Science* (80-. ). 343 (2014) 1210–1211. https://doi.org/10.1126/science.1249625.  
16  
17 [8] A. González, E. Goikolea, J.A. Barrena, R. Mysyk, Review on supercapacitors:  
18 Technologies and materials, *Renew. Sustain. Energy Rev.* 58 (2016) 1189–1206.  
19 https://doi.org/10.1016/j.rser.2015.12.249.  
20  
21 [9] C. Liu, F. Li, M. Lai-Peng, H.M. Cheng, Advanced materials for energy storage, *Adv.*  
22 *Mater.* 22 (2010) 23–26. https://doi.org/10.1002/adma.200903328.  
23  
24 [10] L. Zhang, X.S. Zhao, Carbon-based materials as supercapacitor electrodes, *Chem. Soc.*  
25 *Rev.* 38 (2009) 2520–2531. https://doi.org/10.1039/b813846j.  
26  
27 [11] W. Gu, G. Yushin, Review of nanostructured carbon materials for electrochemical  
28 capacitor applications: Advantages and limitations of activated carbon, carbide-derived  
29 carbon, zeolite-templated carbon, carbon aerogels, carbon nanotubes, onion-like carbon,  
30 and graphene, *Wiley Interdiscip. Rev. Energy Environ.* 3 (2014) 424–473.  
31 https://doi.org/10.1002/wene.102.  
32  
33 [12] V. Augustyn, P. Simon, B. Dunn, Pseudocapacitive oxide materials for high-rate  
34 electrochemical energy storage, *Energy Environ. Sci.* 7 (2014) 1597–1614.  
35 https://doi.org/10.1039/c3ee44164d.  
36  
37 [13] N.R. Chodankar, D.P. Dubal, S.H. Ji, D.H. Kim, Highly efficient and stable negative  
38 electrode for asymmetric supercapacitors based on graphene/FeCo<sub>2</sub>O<sub>4</sub> nanocomposite  
39 hybrid material, *Electrochim. Acta* 295 (2019) 195–203.  
40 https://doi.org/10.1016/j.electacta.2018.10.125.  
41  
42 [14] N.R. Chodankar, D.P. Dubal, Y. Kwon, D.H. Kim, Direct growth of feCo<sub>2</sub>O<sub>4</sub> nanowire  
43 arrays on flexible stainless steel mesh for high-performance asymmetric supercapacitor,  
44 *NPG Asia Mater.* 9 (2017) 1–10. https://doi.org/10.1038/am.2017.145.  
45  
46  
47  
48  
49  
50  
51  
52  
53  
54  
55  
56  
57  
58  
59  
60  
61  
62  
63  
64  
65

[15] C. Yuan, H. Bin Wu, Y. Xie, X.W. Lou, Mixed transition-metal oxides: Design, synthesis, and energy-related applications, *Angew. Chemie - Int. Ed.* 53 (2014) 1488–1504. <https://doi.org/10.1002/anie.201303971>.

[16] F. Zhu, Y. Liu, M. Yan, W. Shi, Construction of hierarchical FeCo<sub>2</sub>O<sub>4</sub>@MnO<sub>2</sub> core-shell nanostructures on carbon fibers for high-performance asymmetric supercapacitor, *J. Colloid Interface Sci.* 512 (2018) 419–427. <https://doi.org/10.1016/j.jcis.2017.09.093>.

[17] Z. Wang, P. Hong, S. Peng, T. Zou, Y. Yang, X. Xing, Z. Wang, R. Zhao, Z. Yan, Y. Wang, Co(OH)<sub>2</sub> @FeCo<sub>2</sub>O<sub>4</sub> as electrode material for high performance faradaic supercapacitor application, *Electrochim. Acta.* 299 (2019) 312–319. <https://doi.org/10.1016/j.electacta.2019.01.017>.

[18] S.G. Mohamed, C.J. Chen, C.K. Chen, S.F. Hu, R.S. Liu, High-performance lithium-ion battery and symmetric supercapacitors based on FeCo<sub>2</sub>O<sub>4</sub> nanoflakes electrodes, *ACS Appl. Mater. Interfaces.* 6 (2014) 22701–22708. <https://doi.org/10.1021/am5068244>.

[19] X. He, R. Li, J. Liu, Q. Liu, R.R. chen, D. Song, J. Wang, Hierarchical FeCo<sub>2</sub>O<sub>4</sub>@NiCo layered double hydroxide core/shell nanowires for high performance flexible all-solid-state asymmetric supercapacitors, *Chem. Eng. J.* 334 (2018) 1573–1583. <https://doi.org/10.1016/j.cej.2017.11.089>.

[20] X. Liu, F. Wei, Y. Sui, J. Qi, Y. He, Q. Meng, Polyhedral ternary oxide FeCo<sub>2</sub>O<sub>4</sub>: A new electrode material for supercapacitors, *J. Alloys Compd.* 735 (2018) 1339–1343. <https://doi.org/10.1016/j.jallcom.2017.11.251>.

[21] X. He, Y. Zhao, R. Chen, H. Zhang, J. Liu, Q. Liu, D. Song, R. Li, J. Wang, Hierarchical FeCo<sub>2</sub>O<sub>4</sub>@polypyrrole Core/Shell Nanowires on Carbon Cloth for High-Performance Flexible All-Solid-State Asymmetric Supercapacitors, *ACS Sustain. Chem. Eng.* 6 (2018) 14945–14954. <https://doi.org/10.1021/acssuschemeng.8b03440>.

[22] B. Pan, J. Xiao, J. Li, P. Liu, C. Wang, G. Yang, Materials: Carbyne with finite length: The one-dimensional sp carbon, *Sci. Adv.* 1 (2015) 1–11. <https://doi.org/10.1126/sciadv.1500857>.

[23] T.C. Dinadayalane, L. Gorb, H. Dodziuk, J. Leszczynski, Modelling of the stabilization of the complex of a single walled (5,5) carbon nanotube C<sub>60</sub>H<sub>20</sub> with cumulenic or acetylenic chain, *AIP Conf. Proc.* 786 (2005) 436–439. <https://doi.org/10.1063/1.2103904>.

[24] B. Zhu, S. Tang, S. Vongehr, H. Xie, X. Meng, Hierarchically MnO<sub>2</sub>-Nanosheet Covered

1  
2  
3  
4 Submicrometer-FeCo<sub>2</sub>O<sub>4</sub>-Tube Forest as Binder-Free Electrodes for High Energy Density  
5 All-Solid-State Supercapacitors, ACS Appl. Mater. Interfaces. 8 (2016) 4762–4770.  
6  
7 https://doi.org/10.1021/acsami.5b11367.  
8  
9

10 [25] A.A. Mirghni, M.J. Madito, K.O. Oyedotun, T.M. Masikhwa, N.M. Ndiaye, S.J. Ray, N.  
11 Manyala, A high energy density asymmetric supercapacitor utilizing a nickel  
12 phosphate/graphene foam composite as the cathode and carbonized iron cations adsorbed  
13 onto polyaniline as the anode, RSC Adv. 8 (2018) 11608–11621.  
14 https://doi.org/10.1039/c7ra12028a.  
15  
16 [26] S. Arunachalam, B. Kirubasankar, V. Murugadoss, D. Vellasamy, S. Angaiah, Facile  
17 synthesis of electrostatically anchored Nd(OH)<sub>3</sub> nanorods onto graphene nanosheets as a  
18 high capacitance electrode material for supercapacitors, New J. Chem. 42 (2018) 2923–  
19 2932. https://doi.org/10.1039/c7nj04335j.  
20  
21 [27] B. Kirubasankar, P. Palanisamy, S. Arunachalam, V. Murugadoss, S. Angaiah, 2D  
22 MoSe<sub>2</sub>-Ni(OH)<sub>2</sub> nanohybrid as an efficient electrode material with high rate capability  
23 for asymmetric supercapacitor applications, Chem. Eng. J. 355 (2019) 881–890.  
24 https://doi.org/10.1016/j.cej.2018.08.185.  
25  
26 [28] N.R. Chodankar, D.P. Dubal, Y. Kwon, D.-H. Kim, Direct growth of FeCo<sub>2</sub>O<sub>4</sub> nanowire  
27 arrays on flexible stainless steel mesh for high-performance asymmetric supercapacitor,  
28 NPG Asia Mater. 9 (2017) e419–e419. https://doi.org/10.1038/am.2017.145.  
29  
30 [29] S.G. Mohamed, S.Y. Attia, H.H. Hassan, Spinel-structured FeCo<sub>2</sub>O<sub>4</sub> mesoporous  
31 nanosheets as efficient electrode for supercapacitor applications, Microporous  
32 Mesoporous Mater. 251 (2017) 26–33. https://doi.org/10.1016/j.micromeso.2017.05.035.  
33  
34 [30] F. Cataldo, A study on the structure and electrical properties of the fourth carbon  
35 allotrope: Carbyne, Polym. Int. 44 (1997) 191–200. https://doi.org/10.1002/(SICI)1097-  
36 0126(199710)44:2<191::AID-PI842>3.0.CO;2-Y.  
37  
38 [31] V.A. Online, B. Duan, W. Wang, A. Wang, K. Yuan, Z. Yu, H. Zhao, J. Qiu, Y. Yang,  
39 lithium / sulfur batteries, (2013) 13261–13267. https://doi.org/10.1039/c3ta12634j.  
40  
41 [32] V.M. Melnitchenko, B.N. Smirnov, V.P. Varlakov, Y.N. Nikulin, A.M. Sladkov, Lamellar  
42 morphology and inner structure of crystalline carbyne fragemnts, Carbon N. Y. 21 (1983)  
43 131–133. https://doi.org/10.1016/0008-6223(83)90168-9.  
44  
45 [33] G. Galeotti, M. Ebrahimi, J. Lipton-Duffin, J.M. Macleod, S. Rondeau-Gagné, J.F. Morin,  
46  
47  
48  
49  
50  
51  
52  
53  
54  
55  
56  
57  
58  
59  
60  
61  
62  
63  
64  
65

1  
2  
3  
4 F. Rosei, 2D Supramolecular networks of dibenzonitrilediacetylene on Ag(111) stabilized  
5 by intermolecular hydrogen bonding, *Phys. Chem. Chem. Phys.* 19 (2017) 10602–10610.  
6  
7 https://doi.org/10.1039/c7cp01058c.  
8  
9 [34] K.V. Sankar, R.K. Selvan, D. Meyrick, Electrochemical performances of CoFe<sub>2</sub>O<sub>4</sub>  
10 nanoparticles and a rGO based asymmetric supercapacitor, *RSC Adv.* 5 (2015) 99959–  
11 99967. https://doi.org/10.1039/c5ra14938j.  
12  
13 [35] S.G. Mohamed, S.Y. Attia, H.H. Hassan, Spinel-structured FeCo<sub>2</sub>O<sub>4</sub> mesoporous  
14 nanosheets as efficient electrode for supercapacitor applications, *Microporous  
15 Mesoporous Mater.* 251 (2017) 26–33. https://doi.org/10.1016/j.micromeso.2017.05.035.  
16  
17 [36] M. Serhan, M. Sprowls, D. Jackemeyer, M. Long, I.D. Perez, W. Maret, N. Tao, E.  
18 Forzani, Total iron measurement in human serum with a smartphone, *AIChE Annu. Meet.*  
19 Conf. Proc. 2019-Novem (2019). https://doi.org/10.1039/x0xx00000x.  
20  
21 [37] L. Lin, S. Tang, S. Zhao, X. Peng, N. Hu, Hierarchical three-dimensional  
22 FeCo<sub>2</sub>O<sub>4</sub>@MnO<sub>2</sub> core-shell nanosheet arrays on nickel foam for high-performance  
23 supercapacitor, *Electrochim. Acta* 228 (2017) 175–182.  
24 https://doi.org/10.1016/j.electacta.2017.01.022.  
25  
26 [38] Q. Wang, X. Wang, J. Xu, X. Ouyang, X. Hou, D. Chen, R. Wang, G. Shen, Flexible  
27 coaxial-type fiber supercapacitor based on NiCo<sub>2</sub>O<sub>4</sub> nanosheets electrodes, *Nano Energy.*  
28 8 (2014) 44–51. https://doi.org/10.1016/j.nanoen.2014.05.014.  
29  
30 [39] L. Abbasi, M. Arvand, Engineering hierarchical ultrathin CuCo<sub>2</sub>O<sub>4</sub> nanosheets array on  
31 Ni foam by rapid electrodeposition method toward high-performance binder-free  
32 supercapacitors, *Appl. Surf. Sci.* 445 (2018) 272–280.  
33  
34 https://doi.org/10.1016/j.apsusc.2018.03.193.  
35  
36  
37  
38  
39  
40  
41  
42  
43  
44  
45  
46  
47  
48  
49  
50  
51  
52  
53  
54  
55  
56  
57  
58  
59  
60  
61  
62  
63  
64  
65

No competing financial interest.